Piezoelectrically Actuated Flextensional Micromachined Ultrasound Transducers—I: Theory

Gökhan Perçin, *Member, IEEE*, and Butrus T. Khuri-Yakub, *Fellow, IEEE*

Abstract—**This series of two papers considers piezoelectrically actuated flextensional micromachined ultrasound transducers (PAFMUTs) and consists of theory, fabrication, and experimental parts. The theory presented in this paper is developed for an ultrasound transducer application presented in the second part. In the absence of analytical expressions for the equivalent circuit parameters of a flextensional transducer, it is difficult to calculate its optimal parameters and dimensions and difficult to choose suitable materials. The influence of coupling between flexural and extensional deformation and that of coupling between the structure and the acoustic volume on the dynamic response of piezoelectrically actuated flextensional transducer are analyzed using two analytical methods: classical thin (Kirchhoff) plate theory and Mindlin plate theory. Classical thin plate theory and Mindlin plate theory are applied to derive two-dimensional plate equations for the transducer and to calculate the coupled electromechanical field variables such as mechanical displacement and electrical input impedance. In these methods, the variations across the thickness direction vanish by using the bending moments per unit length or stress resultants. Thus, two-dimensional plate equations for a step-wise laminated circular plate are obtained as well as two different solutions to the corresponding systems. An equivalent circuit of the transducer is also obtained from these solutions.**

I. Introduction

THE TRANSDUCER design is based on a flextensional transducer that excites the axisymmetric resonant modes of a clamped circular plate. It is constructed by depositing a thin piezoelectric annular plate onto a thin, edge-clamped, circular plate as shown in Fig. 1. An ac voltage is applied across the piezoelectric material to set the compound plate into flexural vibration. We fabricated micromachined piezoelectrically actuated flextensional transducers in a two-dimensional array by combining conventional integrated circuit (IC) manufacturing process technology with ZnO deposition [1]. Individual array elements, shown in Fig. 1, consist mainly of a circular plate attached to an annular disk of piezoelectric material, which has optimized dimensions. The arrays are made by using silicon micromachining techniques and are capable of operation at high frequencies as well as low frequencies. Inherently, this approach offers the advantage of integrating transducers with transmitter and receiver electronics. Thus, we present arrays in which elements can be individually addressed for ease of scanning and focusing by using onboard electronics. To date, however, flextensional tranducers have not been used in ultrasonic applications because of their low frequency response (less than 100 kHz). Here, we present micromachined two-dimensional array flextensional unimorph ultrasonic tranducers that have typical operating resonance frequencies starting from 450 kHz to 4.5 MHz in air. Micromachined small dimensions such as diameter of the vibrating plate and depositing thin films result in higher frequency response along with increased reproducibility.

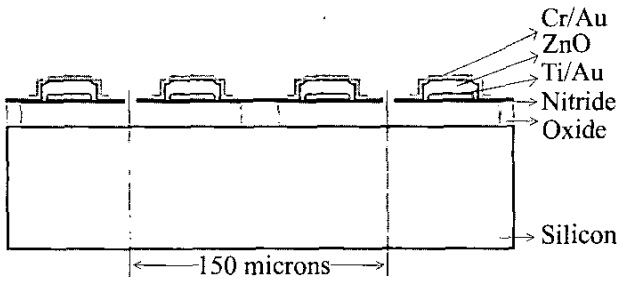

Fig. 1. Configuration of the micromachined flextensional transducer.

The transducer is designed to have maximum volume displacement of the plate at the resonant frequency. Analyses of similar devices such as those of Germano [2], Denkmann *et al.* [3], Allaverdiev *et al.* [4], Vassergiser *et al.* [5], Antonyak *et al.* [6], Brailov *et al.* [7], Adelman *et al.* [8], Okada *et al.* [9], Aronov *et al.* [10], [11], Rosato [12], Greenberg *et al.* [13], Stavsky *et al.* [14], and Rudgers [15] were helpful in identifying the important parameters of the device. However, the complexity of the structure and the fact that the piezoelectric used is an annular disk rather than a full disk necessitates the use of a more complicated analysis to determine the resonant frequencies of the structure, the input impedance of the transducer, and the normal displacement of the surface.

Manuscript received April 23, 2001; accepted November 12, 2001. This research was supported by the Defense Advanced Research Projects Agency of the Department of Defense and was monitored by the Air Force Office of Scientific Research under Grant No. F49620-95-1-0525. This work made use of the National Nanofabrication Users Network facilities funded by the National Science Foundation under award number ECS-9731294.

G. Perçin is with ADEPTIENT, Los Altos, CA 94024 (e-mail: percin@adeptient.com).

B. T. Khuri-Yakub is with Edward L. Ginzton Laboratory, Stanford University, Stanford, CA 94305-4085.

II. Three-Dimensional Coupled Electromechanical System

Because we are interested here in obtaining plate differential equations for axisymmetric vibrations only, we consider the problem in cylindrical coordinates. The linear piezoelectric strain constitutive relations that provide the coupling between the mechanical and electrical fields are given by

$$S_I = d_{Ij}E_j + s^E_{IJ}T_j \quad D_i = \epsilon^T_{ij}E_j + d_{iJ}T_J \tag{1}$$

where T_J, S_I, D_i, and E_j are the components of stress, strain, electric displacement, and electric field, respectively. Material properties are the elastic compliance constants (zero electric field) s^E_{IJ}, the piezoelectric strain constants $d_{Ij} = d_{jI}$, and the dielectric permittivity (zero stress) ϵ^T_{ij}. In addition to these relations, there are two basic field equations, the equation of motion and the strain-mechanical displacement relation,

$$\nabla \cdot \mathbf{T} = \rho \frac{\partial^2 \vec{\mathbf{u}}}{\partial \mathbf{t^2}} \quad \mathbf{S} = \nabla_{\mathbf{S}}\vec{\mathbf{u}}, \tag{2}$$

where ρ is the mass density and $\vec{\mathbf{u}}$ is the mechanical displacement. Because most piezoelectric materials have hexagonal symmetry, this paper contains the solutions for the hexagonal and isotropic systems. The reader should note that these methods can be applied to other geometries in different coordinate systems. Note that $[s_{IJ}]$, $[d_{iJ}]$, and $[\epsilon_{ij}]$ matrices in cylindrical coordinates are the same as those in rectangular coordinates in the case of hexagonal and isotropic systems, i.e., $d_{r5} = d_{x5}$ and $\epsilon^T_{rr} = \epsilon^T_{xx}$. Finally, the linear piezoelectric strain constitutive relations for a hexagonal system can be written as

$$\begin{aligned}
S_{rr} &= s^E_{11}T_{rr} + s^E_{12}T_{\phi\phi} + s^E_{13}T_{zz} + d_{z1}E_z \\
S_{\phi\phi} &= s^E_{12}T_{rr} + s^E_{11}T_{\phi\phi} + s^E_{13}T_{zz} + d_{z1}E_z \\
S_{zz} &= s^E_{13}T_{rr} + s^E_{13}T_{\phi\phi} + s^E_{33}T_{zz} + d_{z3}E_z \\
2S_{\phi z} &= s^E_{44}T_{\phi z} + d_{r5}E_\phi \\
2S_{rz} &= s^E_{44}T_{rz} + d_{r5}E_r \\
2S_{r\phi} &= 2(s^E_{11} - s^E_{12})T_{r\phi} \\
D_r &= \epsilon^T_{rr}E_r + d_{r5}T_{rz} \\
D_\phi &= \epsilon^T_{rr}E_\phi + d_{r5}T_{\phi z} \\
D_z &= \epsilon^T_{zz}E_z + d_{z1}T_{rr} + d_{z1}T_{\phi\phi} + d_{z3}T_{zz}.
\end{aligned} \tag{3}$$

In the presence of mechanical losses, c^E_{IJ}s are complex numbers and will be replaced by $c^E_{IJ} + j\omega\eta^E_{IJ}$. The corresponding s^E_{IJ}s can be found by inverting the c^E_{IJ} matrix. In the presence of electrical losses, ϵ^T_{ij}s are also complex numbers. As a result of these complex representations, there will not be any change in the analysis developed in the following sections.

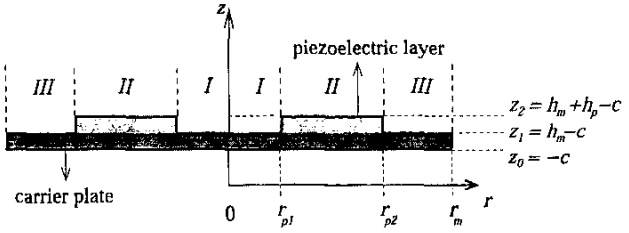

Fig. 2. The geometry of the device.

III. Step-Wise Laminated Plate Analysis

In classical linear thin (Kirchhoff) plate theory, there are a number of assumptions that are necessary to reduce the three-dimensional equations to a two-dimensional set that can be solved. The basic assumptions made in the derivation of the equations for the bending of thin plates are S_{zz} is zero, which in turn means that the transverse deflection w is a function of r and ϕ only. Therefore, S_{zz} will be neglected in three-dimensional coupled electromechanical equations. Moreover, S_{rz} and $S_{\phi z}$ are zero, and T_{zz} is also zero in the stress-strain relations.

In addition, for the flexurally vibrated circular plate, we assume the thickness to be so small that the change of stress is negligible along the z direction. Because the stresses are zero on both surfaces, we can set

$$T_{zz} = T_{rz} = T_{\phi z} = 0. \tag{4}$$

Furthermore, because the motion is entirely in z and radial directions,

$$u_\phi = 0 \quad \text{and} \quad T_{r\phi} = 0. \tag{5}$$

For the region II shown in Fig. 2, because a field is applied only along the z direction,

$$D_r = D_\phi = 0 \quad \text{and} \quad E_r = E_\phi = 0. \tag{6}$$

The remaining coupled electromechanical equations in (3) then become

$$\begin{aligned}
S_{rr} &= s^E_{11}T_{rr} + s^E_{12}T_{\phi\phi} + d_{z1}E_z \\
S_{\phi\phi} &= s^E_{12}T_{rr} + s^E_{11}T_{\phi\phi} + d_{z1}E_z \\
D_z &= d_{z1}T_{rr} + d_{z1}T_{\phi\phi} + \epsilon^T_{zz}E_z
\end{aligned} \tag{7}$$

where

$$S_{rr} = \frac{\partial u_r}{\partial r} \quad \text{and} \quad S_{\phi\phi} = \frac{1}{r}u_r. \tag{8}$$

Because T_{rz} and E_r are zero, transverse shear deformation S_{rz} is also zero, i.e.,

$$S_{rz} = \frac{1}{2}\left(\frac{\partial u_r}{\partial z} + \frac{\partial u_z}{\partial r}\right) = 0.$$

Therefore, the classical kinematic relationships for the flexural motion of the plate are obtained as follows:

$$u_z = w(r,t) \quad \text{and} \quad u_r = -z\frac{\partial w}{\partial r}. \tag{9}$$

By using the previous equations, we obtain the following for the piezoelectric material:

$$T_{rr}^{p} = -z\frac{E_p}{1-\sigma_p^2}\left(\frac{\partial^2 w}{\partial r^2}+\sigma_p\frac{1}{r}\frac{\partial w}{\partial r}\right)-\frac{d_{z1}E_p}{1-\sigma_p}E_z,$$
$$T_{\phi\phi}^{p} = -z\frac{E_p}{1-\sigma_p^2}\left(\sigma_p\frac{\partial^2 w}{\partial r^2}+\frac{1}{r}\frac{\partial w}{\partial r}\right)-\frac{d_{z1}E_p}{1-\sigma_p}E_z, \tag{10}$$

and

$$D_z = -z\frac{d_{z1}E_p}{1-\sigma_p}\left(\frac{\partial^2 w}{\partial r^2}+\frac{1}{r}\frac{\partial w}{\partial r}\right)+\epsilon_{zz}^{T}(1-k_p^2)E_z \tag{11}$$

where $s_{11p} = s_{11}^{E}$, $s_{12p} = s_{12}^{E}$, k_p is the planar coupling factor, E_p is Young's modulus, σ_p is Poisson's ratio, and

$$k_p^2 = \frac{2d_{z1}^2E_p}{\epsilon_{zz}^{T}(1-\sigma_p)} \quad E_p = \frac{1}{s_{11p}} \quad \sigma_p = -\frac{s_{12p}}{s_{11p}}.$$

Moreover, the electric field variables have the following relationships:

$$\nabla.D = 0 \quad \text{i.e.,} \quad D_{z,z} = 0,$$
$$\text{and} \quad -\int_{z_1}^{z_2} E_z\,dz = Ve^{j\omega t}. \tag{12}$$

Similar equations for the non-piezoelectric carrier plate can be derived as follows:

$$T_{rr}^{m} = -z\frac{E_m}{1-\sigma_m^2}\left(\frac{\partial^2 w}{\partial r^2}+\sigma_m\frac{1}{r}\frac{\partial w}{\partial r}\right)$$
$$T_{\phi\phi}^{m} = -z\frac{E_m}{1-\sigma_m^2}\left(\sigma_m\frac{\partial^2 w}{\partial r^2}+\frac{1}{r}\frac{\partial w}{\partial r}\right). \tag{13}$$

For the regions I and III shown in Fig. 2, the bending moments per unit length are given by

$$M_r^{I} = \int_{-h_m/2}^{h_m/2} T_{rr}^{m} z\,dz \quad M_\phi^{I} = \int_{-h_m/2}^{h_m/2} T_{\phi\phi}^{m} z\,dz. \tag{14}$$

For the region II, the bending moments per unit length are given by

$$M_r^{II} = \int_{z_1}^{z_2} T_{rr}^{p} z\,dz + \int_{z_0}^{z_1} T_{rr}^{m} z\,dz$$
$$M_\phi^{II} = \int_{z_1}^{z_2} T_{\phi\phi}^{p} z\,dz + \int_{z_0}^{z_1} T_{\phi\phi}^{m} z\,dz. \tag{15}$$

By substituting in the previous equations while assuming an $e^{j\omega t}$ time dependence, the bending moments per unit length for regions I and III are obtained in terms of the curvatures and the deflection as follows:

$$M_r^{I} = -D_I\left(\frac{d^2W}{dr^2}+\sigma_m\frac{1}{r}\frac{dW}{dr}\right)$$
$$M_\phi^{I} = -D_I\left(\sigma_m\frac{d^2W}{dr^2}+\frac{1}{r}\frac{dW}{dr}\right) \tag{16}$$

where

$$D_I = \frac{h_m^3E_m}{12(1-\sigma_m^2)} \tag{17}$$

is the flexural rigidity of regions I and III. In a similar way, the bending moments per unit length for region II are obtained in terms of the curvatures, the deflection, and the excitation voltage as follows:

$$M_r^{II} = -D_{II}\left(\frac{d^2W}{dr^2}+\sigma_{II}\frac{1}{r}\frac{dW}{dr}\right)-\frac{d_{z1}E_pV(z_2+z_1)}{2(1-\sigma_p)}$$
$$M_\phi^{II} = -D_{II}\left(\sigma_{II}\frac{d^2W}{dr^2}+\frac{1}{r}\frac{dW}{dr}\right)-\frac{d_{z1}E_pV(z_2+z_1)}{2(1-\sigma_p)} \tag{18}$$

where D_{II} and σ_{II} are the flexural rigidity and the equivalent Poisson's ratio for region II, respectively.

The equation of motion for the axisymmetric vibrations takes the following form:

$$T_{rr,r}+\frac{1}{r}(T_{rr}-T_{\phi\phi})+T_{rz,z} = -\rho\omega^2U_r \approx 0$$
$$T_{zz,z}+T_{rz,r}+\frac{T_{rz}}{r} = -\rho\omega^2U_z. \tag{19}$$

The term $\rho\omega^2U_r$, inplane radial inertia, can be neglected. This quasi-static approximation is not valid at higher frequencies. By using the equation of motion, we obtain the following for regions I and III:

$$\nabla^4W_I-\frac{P}{D_I}-\frac{\omega^2W_IR_{0_I}}{D_I} = 0 \tag{20}$$

where $R_{0_I} = \rho_mh_m$ and $[T_{zz}]_{<z>} = P$, where $Pe^{j\omega t}$ is the pressure difference between top and bottom surfaces of the plate. Note that the plate can tell only the difference between normal tractions on the upper and lower surfaces as a result of this analysis. Similar expressions can be found for region II as follows:

$$\nabla^4W_{II}-\frac{P}{D_{II}}-\frac{\omega^2W_{II}R_{0_{II}}}{D_{II}} = 0 \tag{21}$$

where $R_{0_{II}} = \rho_ph_p+\rho_mh_m$. D_I and D_{II} are the corresponding flexural rigidities for the single-layered regions (I and III) and the multi-layered region (II), respectively. As a result, (20) and (21) take the following forms:

$$\left(\nabla^2+k_I^2\right)\left(\nabla^2-k_I^2\right)W_I-\frac{P}{D_I} = 0$$
$$\left(\nabla^2+k_{II}^2\right)\left(\nabla^2-k_{II}^2\right)W_{II}-\frac{P}{D_{II}} = 0 \tag{22}$$

where $k_I^2 = \omega\sqrt{\frac{R_{0_I}}{D_I}}$, $k_{II}^2 = \omega\sqrt{\frac{R_{0_{II}}}{D_{II}}}$, and $\nabla^2 = \frac{d^2}{dr^2}+\frac{1}{r}\frac{d}{dr} = \frac{1}{r}\frac{d}{dr}\left(r\frac{d}{dr}\right)$. Solutions to (22) are in the following

forms:

$$\begin{aligned} W_I &= A_1 J_0(k_I r) + C_1 I_0(k_I r) - \frac{P}{\omega^2 R_{0_I}} \\ W_{II} &= A_2 J_0(k_{II} r) + B_2 Y_0(k_{II} r) + C_2 I_0(k_{II} r) \\ &\quad + D_2 K_0(k_{II} r) - \frac{P}{\omega^2 R_{0_{II}}} \\ W_{III} &= A_3 J_0(k_I r) + B_3 Y_0(k_I r) + C_3 I_0(k_I r) \\ &\quad + D_3 K_0(k_I r) - \frac{P}{\omega^2 R_{0_I}} \end{aligned} \tag{23}$$

with the boundary conditions of

$$\begin{aligned} W_{III} &= 0 & W_{III,r} &= 0 & &\text{at } r = r_m \\ W_{II} &= W_{III} & W_{II,r} &= W_{III,r} & &\text{at } r = r_{p_2} \\ M_r^{II} &= M_r^{III} & Q_r^{II} &= Q_r^{III} & &\text{at } r = r_{p_2} \\ W_{II} &= W_I & W_{II,r} &= W_{I,r} & &\text{at } r = r_{p_1} \\ M_r^{II} &= M_r^I & Q_r^{II} &= Q_r^I & &\text{at } r = r_{p_1} \end{aligned}$$

where $Q_r^i = \int_{<z>_i} T_{rz} dz$ for $i = I, II, III$. Note that, because Y and K tend to infinity as r tends to zero, and W_I is finite at the center of the plate, W_I does not contain terms with Y and K. In addition, these boundary conditions represent a clamped-edge boundary condition. $W_{III} = 0$ and $M_r^{III} = 0$ are set for a simply supported edge boundary condition. $Q_r^{III} = 0$ and $M_r^{III} = 0$ are set for a free edge boundary condition. In the presence of mechanical losses, k_I and k_{II} are complex numbers. Because the functions $J_n(kr)$, $Y_n(kr)$, $I_n(kr)$, and $K_n(kr)$ can have complex variables, the previously mentioned formulation does not have any change. Solutions to (22) can be generalized to step-wise multiple layer laminated annular plates. For example, the geometry of the transducer may also contain the top and bottom electrode layers; or, equivalently, region II may also contain the top and bottom electrode layers; and region I may also contain a hole.

A. Equivalent Circuit

The electro-acoustic two-port network equations corresponding to the network in Fig. 3 can be written in the following form:

$$\begin{aligned} I &= y_{11} V + y_{12} P \\ \overline{v} &= y_{21} V + y_{22} P \end{aligned} \tag{24}$$

where I is the electric displacement current on the piezoelectric material, $\overline{v}$ is the volume velocity of the vibrating plate, V is the electric voltage across the piezoelectric material, P is the pressure applied to the transducer, and $\overline{Z}_L$ is the acoustical load impedance caused by the radiation from a vibrating plate.

To study the electro-acoustical efficiency, the equivalent circuit of the transducer shown in Fig. 4 is used, where Z_A is the acoustical impedance of the transducer, C_0 is the clamped electrical capacitance of the compound plate, and N_A is the electroacoustical conversion efficiency.

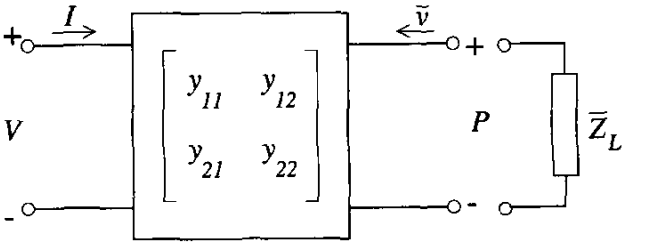

Fig. 3. Equivalent two-port network.

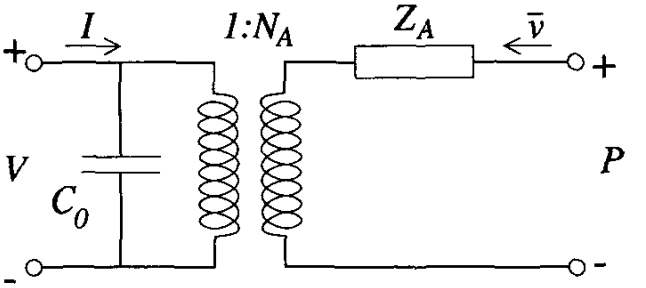

Fig. 4. Equivalent circuit.

The electric displacement current in the piezoelectric material, I, is given by

$$I = j2\pi\omega \int_{r_{p1}}^{r_{p2}} D_z r dr. \tag{25}$$

The volume velocity of the vibrating plate, $\overline{v}$, is given by

$$\overline{v} = j2\pi\omega \left[\int_0^{r_{p1}} W_I r dr + \int_{r_{p1}}^{r_{p2}} W_{II} r dr + \int_{r_{p2}}^{r_m} W_{III} r dr \right]. \tag{26}$$

The equivalent circuit and expressions for calculating its parameters can be used to estimate the input impedance, the sensitivity, the efficiency, and a number of other characteristics of the transducer. For example, the input impedance of the transducer is given by

$$Z_{in} = \frac{V}{I} = \frac{y_{22}\overline{Z}_L + 1}{y_{11} + \overline{Z}_L (y_{11} y_{22} - y_{12} y_{21})} \tag{27}$$

where $\overline{Z}_L = \frac{Z_a}{S_T}$, Z_a is the acoustical impedance of the medium, and $S_T = \pi r_m^2$ is the surface area of the transducer. In these equations, the radiation impedance of a circular piston should be used for $\overline{Z}_L$ to obtain more accurate results.

IV. Application of Mindlin Plate Theory

It is well known that the classical thin plate theory satisfactorily predicts actual behavior only for the first few flexural modes of motion of a plate whose thickness is small

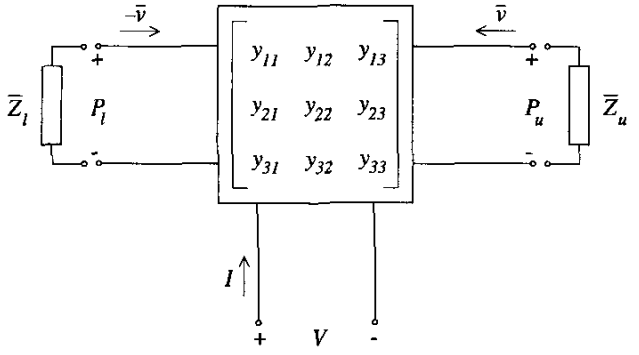

Fig. 5. Equivalent three-port network.

TABLE I
PHYSICAL DIMENSIONS OF THE SIMULATED LARGE-SCALE DEVICE.

Dimension	Value
Radius of brass carrier plate	4 mm
Inner radius of piezoelectric Murata SW material	1 mm
Outer radius of piezoelectric Murata SW material	3 mm
Thickness of brass carrier plate	25 μm
Thickness of piezoelectric Murata SW Material	20 μm

compared with its lateral dimensions. For the higher flexural modes, the influence of coupling to the thickness-shear mode of motion becomes increasingly important. Hence, the classical theory, in which this effect is neglected, ceases to yield reliable information. The assumption of the classical theory regarding normals to the neutral remaining normal to the deformed plane amounts to neglecting the effect of transverse shear deformation. This effect, together with the rotatory inertia (or inplane radial inertia) effect, becomes important when the plate is relatively thick or when accurate solutions for higher modes of vibration are desired. To allow for the effect of transverse shear deformation, the theory relaxes the normality assumption so that normals to the undeformed neutral plane remain straight and unstretched in length but not necessarily normal to the deformed neutral plane. This assumption implies a nonzero transverse shear strain, but it also leads to the statical violation of zero shear stress at the free surfaces because the shear stress becomes constant through the plate thickness. To compensate for this error, Mindlin [16] proposed a shear correction factor to be applied to the shear force. Besides, Mindlin modified the sixth assumption so that the effect of rotatory inertia (or inplane radial inertia) is included. Thus, the influence of coupling between flexure and shear is taken into account by inclusion of rotatory inertia (or inplane radial inertia) and shear deformation terms in the equations. Mindlin plate theory is further modified by including T_{zz} in the equations to consider the relatively large pressure difference between upper and lower surfaces of the plate. In the Mindlin plate theory, the displacement components are assumed to be given by

$$u_r = z\,u(r,t) \quad u_z = w(r,t). \tag{28}$$

$u(r,t)$ can be thought of as the local rotation (change of slope) in the r direction of lines originally normal to the neutral plane before deformation. That is, the rotation $u(r,t)$ is due to bending. The deflection of the neutral plane $w(r,t)$ is then composed of two parts: one caused by bending and the other caused by shear deformation. The remaining coupled electromechanical equations in (3) then become

$$\begin{aligned} S_{rr} &= s_{11}^E T_{rr} + s_{12}^E T_{\phi\phi} + s_{13}^E T_{zz} + d_{z1} E_z \\ S_{\phi\phi} &= s_{12}^E T_{rr} + s_{11}^E T_{\phi\phi} + s_{13}^E T_{zz} + d_{z1} E_z \\ 2S_{rz} &= s_{44}^E T_{rz} \\ D_z &= \epsilon_{zz}^T E_z + d_{z1} T_{rr} + d_{z1} T_{\phi\phi} + d_{z3} T_{zz} \end{aligned} \tag{29}$$

where

$$\begin{aligned} S_{rr} &= \frac{\partial u_r}{\partial r}, \quad S_{\phi\phi} = \frac{1}{r} u_r, \quad \text{and} \\ S_{rz} &= \frac{1}{2}\left(\frac{\partial u_r}{\partial z} + \frac{\partial u_z}{\partial r}\right). \end{aligned} \tag{30}$$

By using the previous equations, we obtain the following for the piezoelectric material:

$$\begin{aligned} T_{rr}^p &= z\frac{E_p}{1-\sigma_p^2}\left(\frac{\partial u}{\partial r} + \sigma_p \frac{1}{r} u\right) - \frac{d_{z1} E_p}{1-\sigma_p} E_z - \frac{s_{13p} E_p}{1-\sigma_p} T_{zz}, \\ T_{\phi\phi}^p &= z\frac{E_p}{1-\sigma_p^2}\left(\sigma_p \frac{\partial u}{\partial r} + \frac{1}{r} u\right) - \frac{d_{z1} E_p}{1-\sigma_p} E_z - \frac{s_{13p} E_p}{1-\sigma_p} T_{zz}, \\ T_{rz}^p &= G_p\left(u + \frac{\partial w}{\partial r}\right), \end{aligned} \tag{31}$$

and

$$D_z = z\frac{d_{z1} E_p}{1-\sigma_p}\left(\frac{\partial u}{\partial r} + \frac{1}{r} u\right) + \epsilon_{zz}^T (1-k_p^2) E_z + \tilde{d}_{z3} T_{zz}. \tag{32}$$

Similar equations can be obtained for the non-piezoelectric material as follows:

$$\begin{aligned} T_{rr}^m &= z\frac{E_m}{1-\sigma_m^2}\left(\frac{\partial u}{\partial r} + \sigma_m \frac{1}{r} u\right) - \frac{s_{13m} E_m}{1-\sigma_m} T_{zz} \\ T_{\phi\phi}^m &= z\frac{E_m}{1-\sigma_m^2}\left(\sigma_m \frac{\partial u}{dr} + \frac{1}{r} u\right) - \frac{s_{13m} E_m}{1-\sigma_m} T_{zz} \\ T_{rz}^m &= G_m\left(u + \frac{\partial w}{\partial r}\right) \end{aligned} \tag{33}$$

TABLE II
PHYSICAL DIMENSIONS OF THE SIMULATED MICROMACHINED DEVICE.

Dimension	Value
Radius of the silicon nitride carrier plate	50 μm
Radius of the orifice	3 μm
Inner radius of piezoelectric zinc oxide	15 μm
Outer radius of piezoelectric zinc oxide	40 μm
Thickness of carrier plate silicon nitride	0.3 μm
Thickness of piezoelectric zinc oxide	0.3 μm
Thickness of gold electrodes	0.1 μm

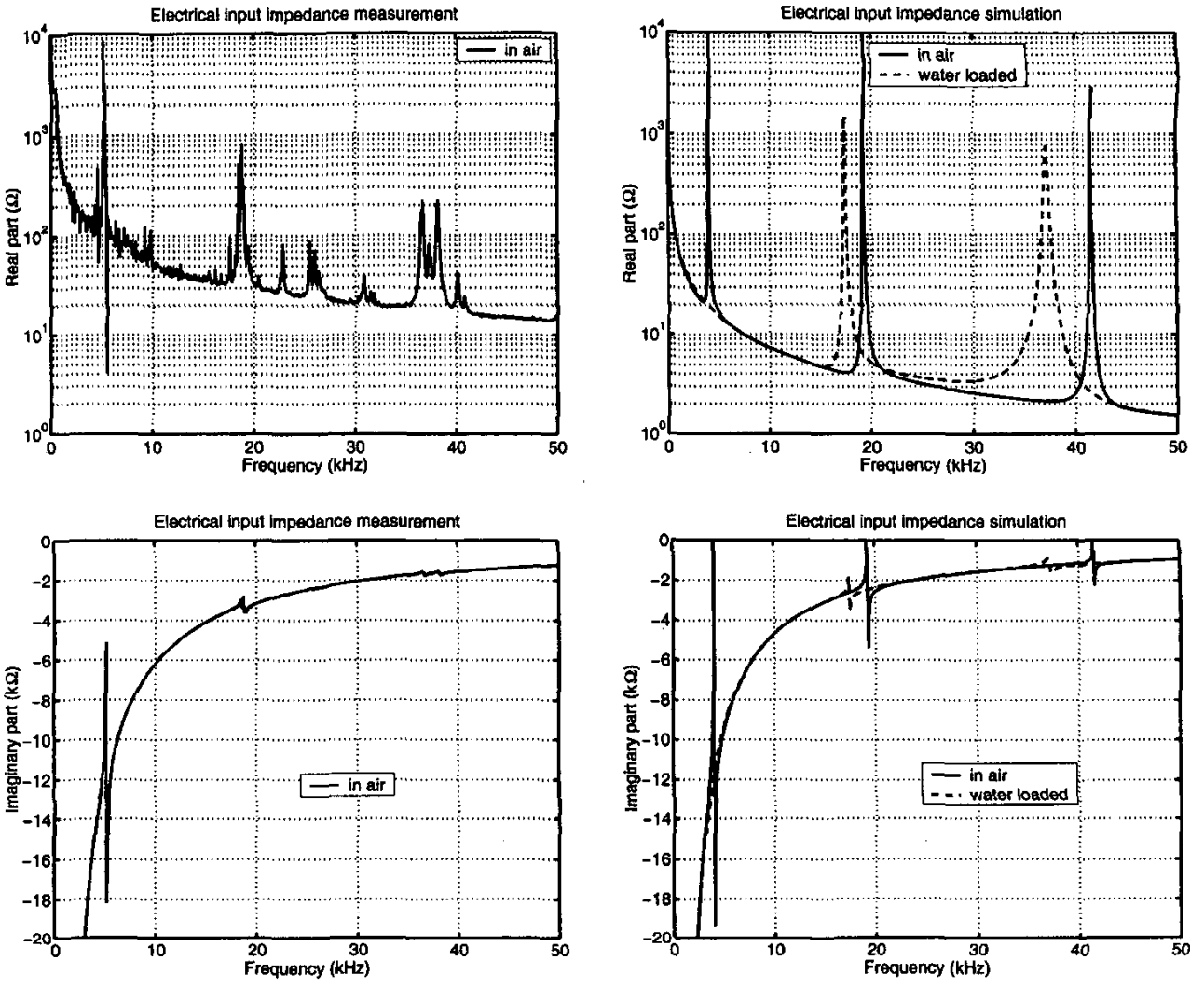

Fig. 6. Large-scale device electrical input impedance measurement and simulation.

where $G_p = \frac{1}{s_{44p}}$ and $G_m = \frac{1}{s_{44m}}$ are the shear moduli,

$$\tilde{d}_{z3} = d_{z3} - \frac{2d_{z1}s_{13p}E_p}{1-\sigma_p},$$

and T_{zz} is approximated by

$$T_{zz} = \frac{z_u P_l - z_l P_u + (P_u - P_l)z}{z_u - z_l}. \tag{34}$$

P_u and P_l are the pressures at the top and bottom surfaces of the plate, respectively, and z_u and z_l are the coordinates of the top and bottom surfaces of the plate, respectively.

By using the previous equations, we obtain the following bending moments per unit length and the transverse shearing forces per unit length for regions I and III:

$$\begin{aligned} M_r^I &= D_I\left(\frac{dU}{dr} + \sigma_m\frac{1}{r}U\right) - F_I \\ M_\phi^I &= D_I\left(\sigma_m\frac{dU}{dr} + \frac{1}{r}U\right) - F_I \\ Q_r^I &= \tilde{g}_I\left(U + \frac{dW}{dr}\right). \end{aligned} \tag{35}$$

In a similar way, we obtain the following for region II

$$\begin{aligned} M_r^{II} &= D_{II}\left(\frac{dU}{dr} + \sigma_{II}\frac{1}{r}U\right) - \frac{d_{z1}E_pV(z_2+z_1)}{2(1-\sigma_p)} - F_{II} \\ M_\phi^{II} &= D_{II}\left(\sigma_{II}\frac{dU}{dr} + \frac{1}{r}U\right) - \frac{d_{z1}E_pV(z_2+z_1)}{2(1-\sigma_p)} - F_{II} \\ Q_r^{II} &= \tilde{g}_{II}\left(U + \frac{dW}{dr}\right) \end{aligned} \tag{36}$$

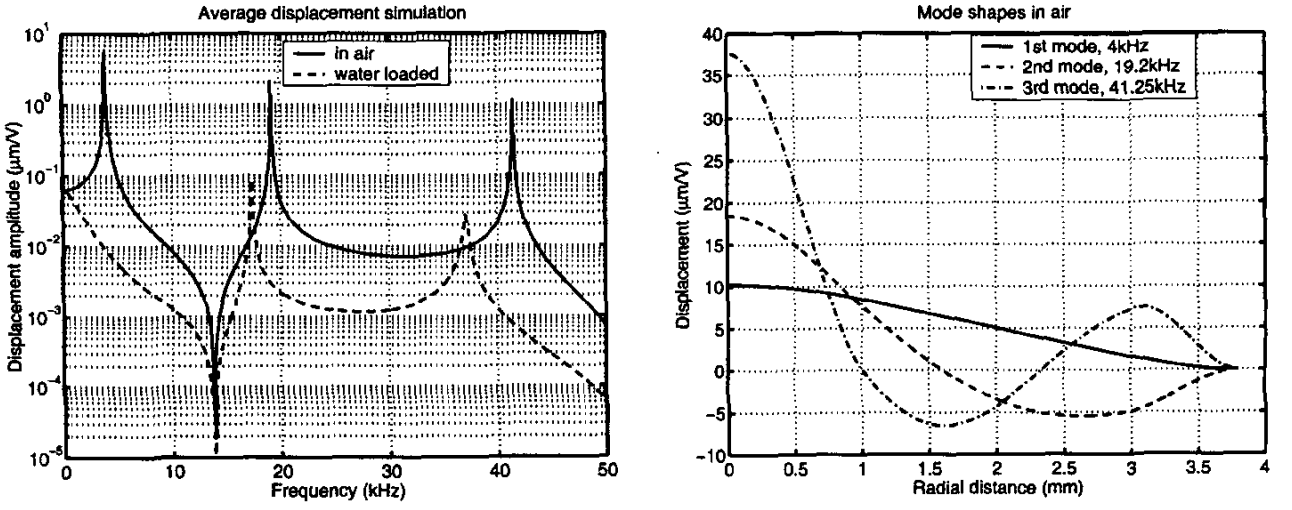

Fig. 7. Large-scale device average displacement and mode shape simulations.

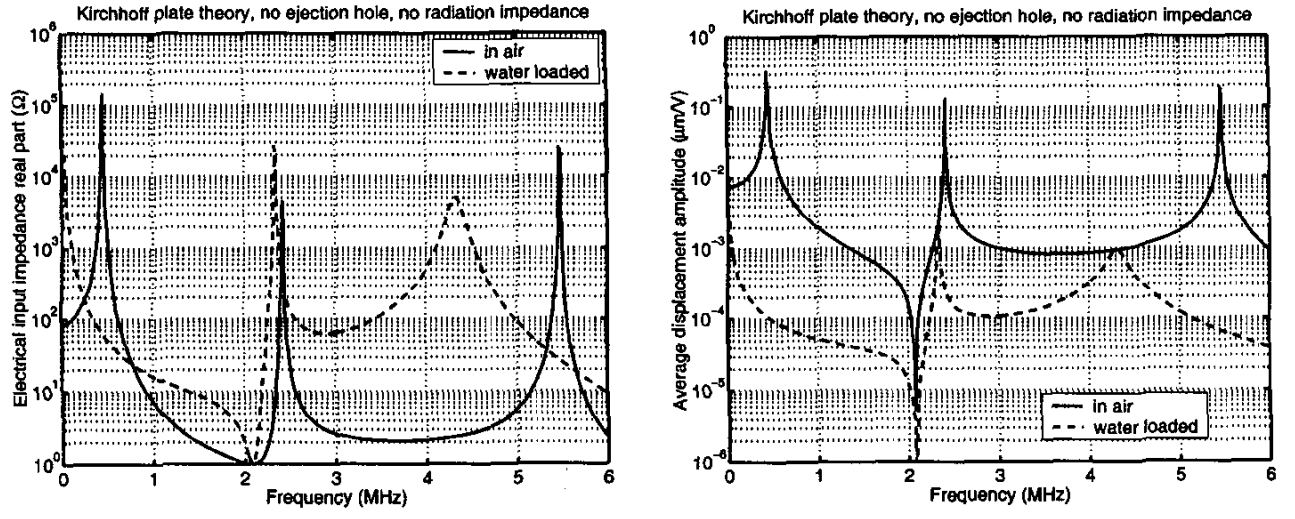

Fig. 8. Simulation example of a micromachined device without ejection hole by using classical thin (Kirchhoff) plate theory and not using radiation impedance.

where

$$F_I = \frac{s_{13m} E_m h_m^2 (P_u - P_l)}{12(1-\sigma_m)},$$

$$F_{II} = \frac{s_{13m} E_m \left[3(z_2 P_l - z_0 P_u)(z_1^2 - z_0^2) + 2(P_u - P_l)(z_1^3 - z_0^3)\right]}{6(1-\sigma_m)(h_m + h_p)} + \frac{s_{13p} E_p \left[3(z_2 P_l - z_0 P_u)(z_2^2 - z_1^2) + 2(P_u - P_l)(z_2^3 - z_1^3)\right]}{6(1-\sigma_p)(h_m + h_p)},$$

and

$$\tilde{g}_I = \kappa^2 G_m h_m, \quad \tilde{g}_{II} = \kappa^2 (G_m h_m + G_p h_p), \quad \kappa^2 = \frac{\pi^2}{12}.$$

κ^2 is the shear correction factor to compensate for the error in assuming a constant shear stress throughout the plate thickness. It is introduced for the dispersion curves to match those of the three-dimensional theory at the thickness-shear frequencies.

The equation of motion can be written as

$$T_{rr,r} + \frac{1}{r}(T_{rr} - T_{\phi\phi}) + T_{rz,z} = -\rho\omega^2 z U$$
$$T_{zz,z} + T_{rz,r} + \frac{T_{rz}}{r} = -\rho\omega^2 W. \tag{37}$$

By using the equation of motion, the differential equation corresponding to the forced flexural vibrations in regions

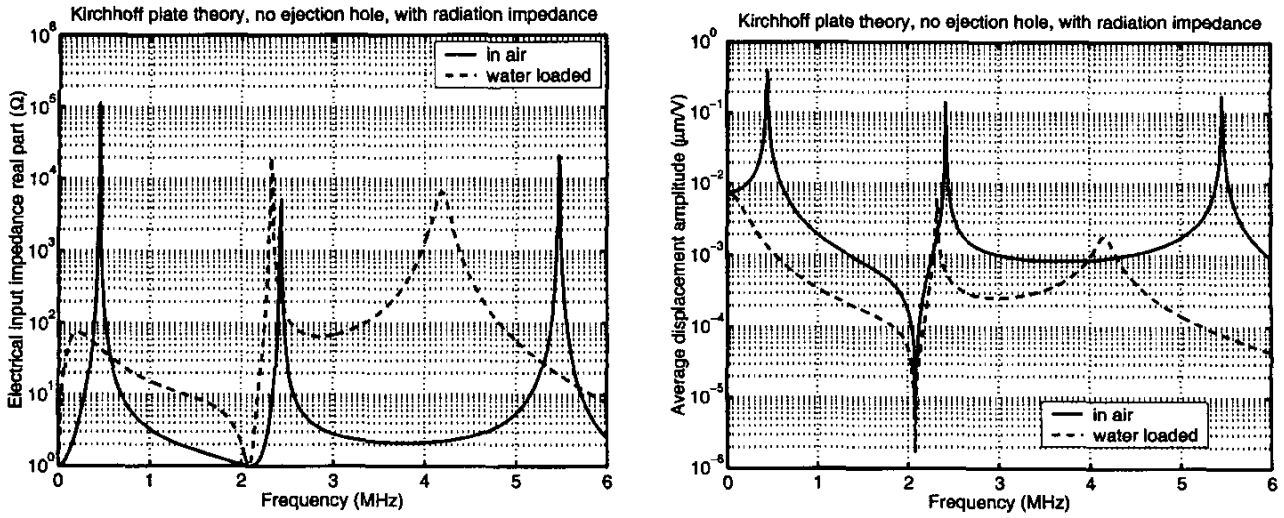

Fig. 9. Simulation example of a micromachined device without ejection hole by using classical thin plate theory and radiation impedance of a circular piston.

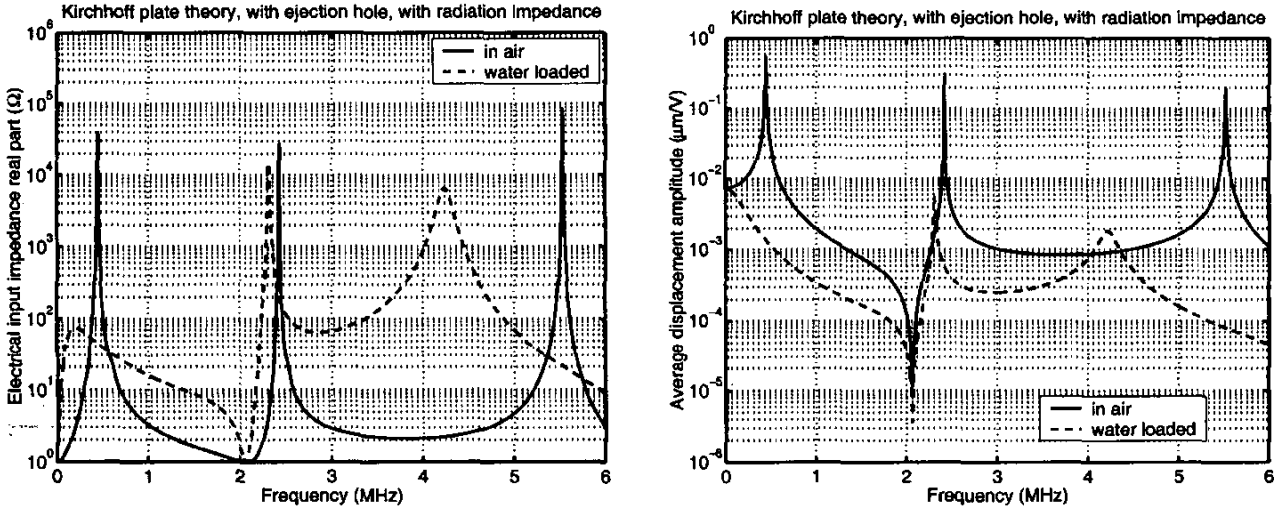

Fig. 10. Simulation example of a micromachined device with 6-μm diameter ejection hole using classical thin plate theory and radiation impedance of a circular piston.

I and III is obtained as follows:

$$\frac{d^4W_I}{dr^4}+\frac{2}{r}\frac{d^3W_I}{dr^3}-\frac{1}{r^2}\frac{d^2W_I}{dr^2}+\frac{1}{r^3}\frac{dW_I}{dr}+\omega^2\left(\frac{R_{0_I}}{\tilde{g}_I}+\frac{R_{2_I}}{D_I}\right)\left(\frac{d^2W_I}{dr^2}+\frac{1}{r}\frac{dW_I}{dr}\right)+\frac{\omega^2R_{2_I}-\tilde{g}_I}{\tilde{g}_ID_I}\left[\omega^2R_{0_I}W_I+(P_u-P_l)\right]=0;$$

or, equivalently, it can be written as

$$\nabla^4W_I+\delta_I^4(R_I+S_I)\nabla^2W_I+\delta_I^4(R_IS_I\delta_I^4-1)W_I+(R_IS_I\delta_I^4-1)\frac{P_u-P_l}{D_I}=0 \quad (38)$$

where

$$\delta_I^4=\frac{\omega^2R_{0_I}}{D_I} \quad S_I=\frac{D_I}{\tilde{g}_I} \quad R_I=\frac{R_{2_I}}{R_{0_I}}$$

$$R_{0_I}=\rho_mh_m \quad R_{2_I}=\frac{\rho_mh_m^3}{12} \quad \nabla^2=\frac{d^2}{dr^2}+\frac{1}{r}\frac{d}{dr}.$$

Eq. (38) can also be written in the following compact form:

$$(\nabla^2+k_I^2)(\nabla^2+l_I^2)W_I+(R_IS_I\delta_I^4-1)\frac{P_u-P_l}{D_I}=0 \quad (39)$$

where

$$k_I^2 = \frac{\delta_I^4}{2}\left[R_I + S_I + \sqrt{(R_I - S_I)^2 + 4\delta_I^{-4}}\right]$$
$$l_I^2 = \frac{\delta_I^4}{2}\left[R_I + S_I - \sqrt{(R_I - S_I)^2 + 4\delta_I^{-4}}\right].$$

The general solution to (39) can be expressed as

$$\begin{aligned} W_I &= W_{I_1} + W_{I_2} - \frac{P_u - P_l}{\omega^2 R_{0_I}} \\ (\nabla^2 + k_I^2)W_{I_1} &= 0 \\ (\nabla^2 + l_I^2)W_{I_2} &= 0. \end{aligned} \tag{40}$$

A similar differential equation corresponding to the forced flexural vibrations in region II is obtained as follows:

$$\nabla^4 W_{II} + \delta_{II}^4(R_{II}+S_{II})\nabla^2 W_{II} + \delta_{II}^4(R_{II}S_{II}\delta_{II}^4 - 1)W_{II} + (R_{II}S_{II}\delta_{II}^4 - 1)\frac{P_u - P_l}{D_{II}} = 0 \tag{41}$$

where

$$\delta_{II}^4 = \frac{\omega^2 R_{0_{II}}}{D_{II}} \quad S_{II} = \frac{D_{II}}{\tilde{g}_{II}} \quad R_{II} = \frac{R_{2_{II}}}{R_{0_{II}}}$$
$$R_{0_{II}} = \rho_m h_m + \rho_p h_p \quad R_{2_{II}} = \frac{\rho_m(z_1^3 - z_0^3) + \rho_p(z_2^3 - z_1^3)}{3}.$$

Eq. (41) can be also written in the following compact form:

$$(\nabla^2 + k_{II}^2)(\nabla^2 + l_{II}^2)W_{II} + (R_{II}S_{II}\delta_{II}^4 - 1)\frac{P_u - P_l}{D_{II}} = 0 \tag{42}$$

where

$$k_{II}^2 = \frac{\delta_{II}^4}{2}\left[R_{II} + S_{II} + \sqrt{(R_{II} - S_{II})^2 + 4\delta_{II}^{-4}}\right]$$
$$l_{II}^2 = \frac{\delta_{II}^4}{2}\left[R_{II} + S_{II} - \sqrt{(R_{II} - S_{II})^2 + 4\delta_{II}^{-4}}\right].$$

The general solution to (42) can be expressed as

$$\begin{aligned} W_{II} &= W_{II_1} + W_{II_2} - \frac{P_u - P_l}{\omega^2 R_{0_{II}}} \\ (\nabla^2 + k_{II}^2)W_{II_1} &= 0 \\ (\nabla^2 + l_{II}^2)W_{II_2} &= 0. \end{aligned} \tag{43}$$

Solutions to (42) and (39) in regions I, II, and III are in the following forms:

$$\begin{aligned} W_I &= A_1 J_0(k_I r) + C_1 J_0(l_I r) - \frac{P_u - P_l}{\omega^2 R_{0_I}} \\ W_{II} &= A_2 J_0(k_{II} r) + B_2 Y_0(k_{II} r) + C_2 J_0(l_{II} r) \\ &\quad + D_2 Y_0(l_{II} r) - \frac{P_u - P_l}{\omega^2 R_{0_{II}}} \\ W_{III} &= A_3 J_0(k_I r) + B_3 Y_0(k_I r) + C_3 J_0(l_I r) \\ &\quad + D_3 Y_0(l_I r) - \frac{P_u - P_l}{\omega^2 R_{0_I}} \end{aligned} \tag{44}$$

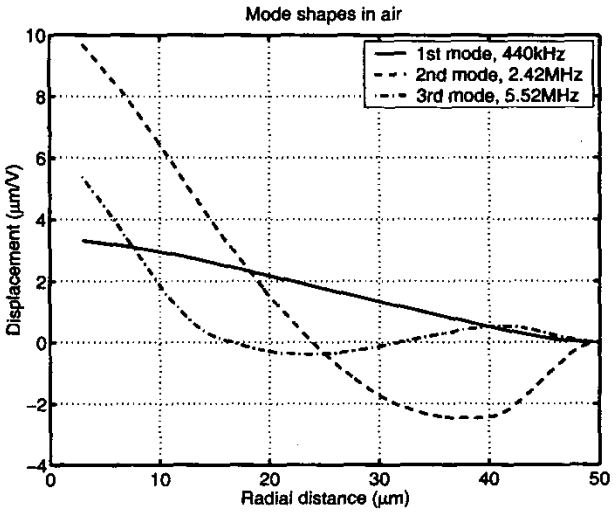

Fig. 11. Simulated mode shapes of a micromachined device with 6-μm diameter ejection hole using classical thin plate theory.

with the boundary conditions of

$$\begin{aligned} W_{III} &= 0 & U_{III} &= 0 & &\text{at } r = r_m \\ W_{II} &= W_{III} & U_{II} &= U_{III} & &\text{at } r = r_{p_2} \\ M_r^{II} &= M_r^{III} & Q_r^{II} &= Q_r^{III} & &\text{at } r = r_{p_2} \\ W_{II} &= W_I & U_{II} &= U_I & &\text{at } r = r_{p_1} \\ M_r^{II} &= M_r^I & Q_r^{II} &= Q_r^I & &\text{at } r = r_{p_1}. \end{aligned}$$

Note that, because Y tends to infinity as r tends to zero and because W_I is finite at the center of the plate, W_I does not contain terms with Y. In addition, these boundary conditions represent a clamped-edge boundary condition; $W_{III} = 0$ and $M_r^{III} = 0$ are set for a simply supported edge boundary condition. $Q_r^{III} = 0$ and $M_r^{III} = 0$ are set for a free-edge boundary condition. In the presence of mechanical losses, k_I, l_I, k_{II}, and l_{II} are complex numbers. Because the functions $J_n(kr)$ and $Y_n(kr)$ can have complex variables, this formulation does not change.

A. Equivalent Circuit

The electro-acoustic three-port network equations corresponding to the network in Fig. 5 can be written in the following form:

$$\begin{aligned} I &= y_{11}V + y_{12}P_u + y_{13}P_l \\ \overline{v} &= y_{21}V + y_{22}P_u + y_{23}P_l \\ -\overline{v} &= y_{31}V + y_{32}P_u + y_{33}P_l \end{aligned} \tag{45}$$

where I is the electric displacement current on the piezoelectric material, $\overline{v}$ is the volume velocity of the vibrating plate, V is the electric voltage across the piezoelectric material, P_u is the pressure applied to the top surface of the transducer, and P_l is the pressure applied to the bottom

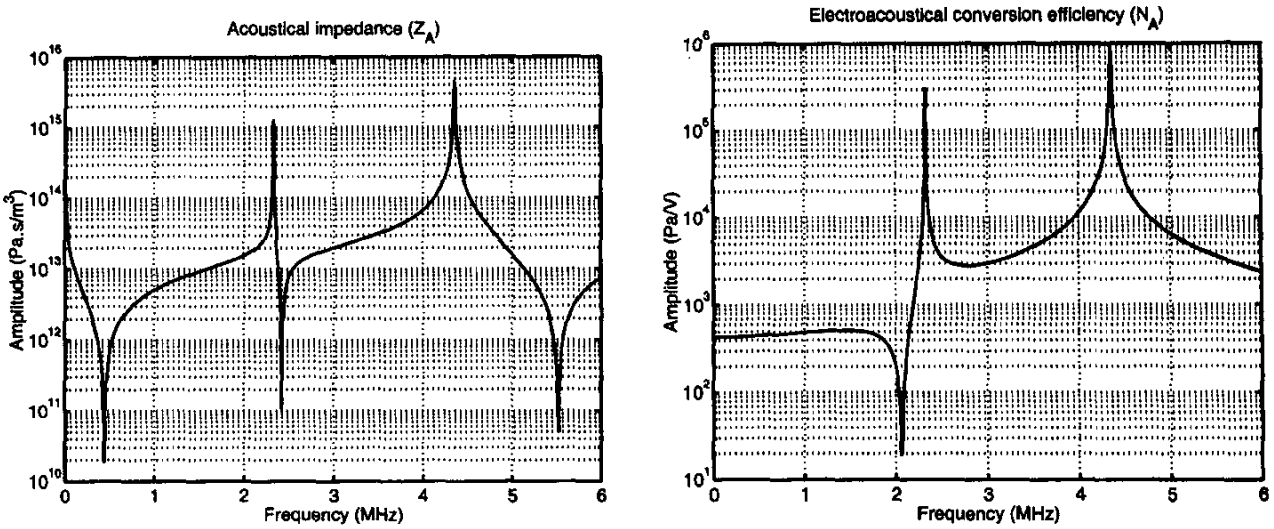

Fig. 12. Simulated equivalent circuit parameters of a micromachined device with 6-μm diameter ejection hole using classical thin plate theory.

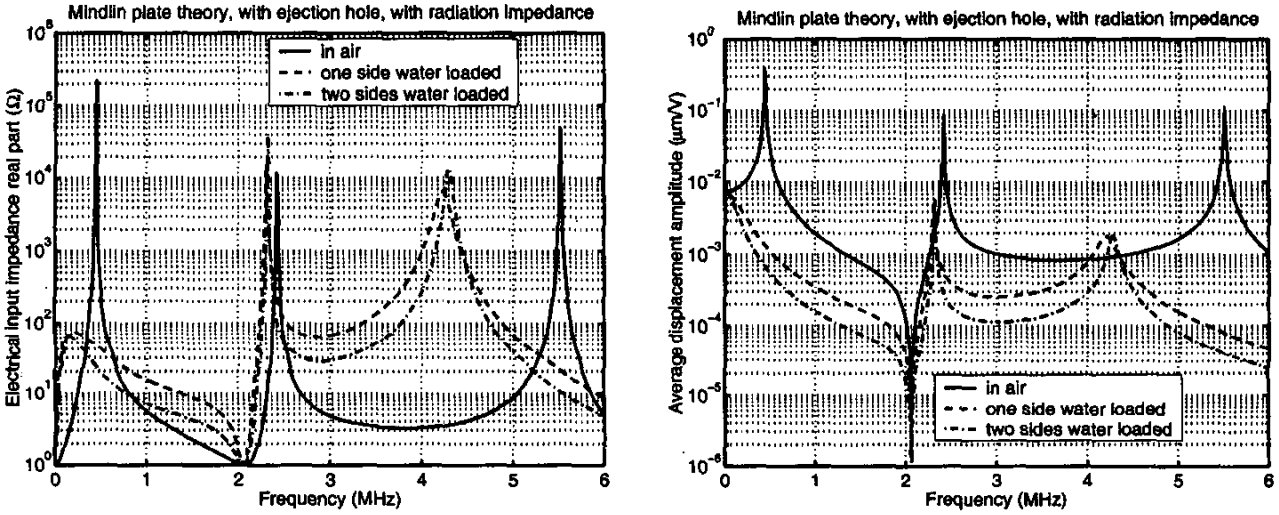

Fig. 13. Simulation example of a micromachined device with 6-μm diameter ejection hole using modified Mindlin plate theory and radiation impedance of a circular piston.

surface of the transducer. Because the motion is entirely flexural, the velocity of the bottom surface of the plate is the negative of the velocity of the top surface. It is clear from the previous equations that $y_{31} = -y_{21}$, $y_{32} = -y_{22}$, and $y_{33} = -y_{23}$. In addition, if the assumption of the classical plate theory, which states that T_{zz} vanishes through the thickness of the plate, is made, then $y_{13} = -y_{12}$ and $y_{23} = -y_{22}$.

The equivalent three-port network and expressions for calculating its parameters can be used to estimate the input impedance, the sensitivity, the efficiency, and a number of other characteristics of the transducer. For example, the input impedance of the transducer is given by

$$Z_{in} = \frac{V}{I} = \frac{1 + y_{22}\overline{Z}_u - y_{23}\overline{Z}_l}{y_{11} + \overline{Z}_u(y_{11}y_{22} - y_{12}y_{21}) - \overline{Z}_l(y_{11}y_{23} - y_{13}y_{21})} \quad (46)$$

where $\overline{Z}_u$ and $\overline{Z}_l$ are the acoustical load impedance of the media that are in contact with the top and bottom surfaces of the transducer, respectively.

V. Simulation Examples

By using the model developed in this paper, the electrical input impedance, average displacement, and mode

shape simulations for large-scale device dimensions and materials given in Table I are presented in Fig. 6 and 7. As shown in Fig. 6, the measured real and imaginary parts of the electrical input impedance resemble those obtained by the model. The model is also capable of predicting electrical input impedance and average displacement of the fluid-loaded device, and the corresponding simulations are also presented in Fig. 6 and 7. As presented in these plots, the resonant frequencies are decreased by fluid loading on one side of the plate.

In the following figures, simulation examples, using the theory developed in this paper, are presented for the micromachined device dimensions, and materials are given in Table II. In Fig. 8, simulation results of a micromachined device without an ejection hole (orifice) by using classical thin (Kirchhoff) plate theory and by not using the radiation impedance definition are given. In Fig. 9, the simulation results of the same configuration, except using the radiation impedance definition, are given. Note that using the radiation impedance definition changes the low frequency response, i.e., it introduces relatively wide band electrical resonance at lower frequencies for the water-loaded case. This is because of the fact that the propagation wavenumber for acoustic waves in water is relatively small. The simulation results in Fig. 10 correspond to the case where the ejection hole is also included in the calculations. Addition of the ejection hole does not change the simulation results significantly, because the radius of the orifice is much smaller compared with the overall radius of the device. In Fig. 11 and 12, the mode shapes, the acoustical impedance, and the electro-acoustical conversion efficiency are shown for the case in Fig. 10. Fig. 13 shows the simulation results by using the modified Mindlin plate theory developed in this paper. These results are given for the cases in which the device operates in air, has one side loaded with water, and has two sides loaded with water. As seen in Fig. 13, the average displacement decreases more in the case of two sides, loaded with water.

VI. Conclusion

In summary, classical thin plate theory and Mindlin plate theory are applied to derive two-dimensional plate equations for the transducer and to calculate the coupled electromechanical field variables such as mechanical displacement. These methods use classical kinematic relations for the coupled electromechanical field to reduce three-dimensional field equations to two-dimensional plate equations. As a result, two different exact solutions to the corresponding systems are obtained. An equivalent circuit of the transducer is also obtained from these solutions.

Acknowledgment

This research was conducted during G. Perçin's Ph.D. study at Stanford University.

References

[1] G. Perçin and B. T. Khuri-Yakub, "Piezoelectrically actuated flextensional micromachined ultrasound transducers—II: Fabrication and Experiments," *IEEE Trans. Ultrason., Ferroelect., Freq. Contr.*, vol. 49, no. 4, pp. 585–595, Apr. 2002.

[2] C. P. Germano, "Flexure mode piezoelectric transducers," *IEEE Trans. Audio Electroacoust.*, vol. AU-19, pp. 6–12, Mar. 1973.

[3] W. J. Denkmann, R. E. Nickell, and D. C. Stickler, "Analysis of structural-acoustic interactions in metal-ceramic transducers," *IEEE Trans. Audio Electroacoust.*, vol. AU-21, no. 4, pp. 317–324, Aug. 1973.

[4] A. M. Allaverdiev, N. B. Akhmedov, and T. D. Shermergor, "Coupled flexural-shear oscillations of stepwise-layered piezoceramic disk transducers," *Sov. Appl. Mech.*, vol. 23, pp. 465–471, May 1987.

[5] M. E. Vassergiser, A. N. Vinnichenko, and A. G. Dorosh, "Calculation and investigation of flexural-mode piezoelectric disk transducers on a passive substrate in reception and radiation," *Sov. Phys. Acoust.*, vol. 38, no. 6, pp. 558–561, Nov.-Dec. 1992.

[6] Y. T. Antonyak and M. E. Vassergiser, "Calculation of the characteristics of a membrane-type flexural-mode piezoelectric transducer," *Sov. Phys. Acoust.*, vol. 28, no. 3, pp. 176–180, May-Jun. 1982.

[7] É. S. Brailov and M. E. Vassergiser, "Estimation of the characteristics of a disk-shaped flexural-mode bimorph cell," *Sov. Phys. Acoust.*, vol. 26, no. 4, pp. 325–328, Jul.-Aug. 1980.

[8] N. T. Adelman and Y. Stavsky, "Flexural-extensional behavior of composite piezoelectric circular plates," *J. Acoust. Soc. Amer.*, vol. 67, no. 3, pp. 819–822, Mar. 1980.

[9] H. Okada, M. Kurosawa, S. Ueha, and M. Masuda, "New airborne ultrasonic transducer with high output sound pressure level," *Jpn. J. Appl. Phys.*, pt. 1, vol. 33, no. 5B, pp. 3040–3044, May 1994.

[10] B. S. Aronov and L. B. Nikitin, "Calculation of the flexural modes of piezoceramic plates," *Sov. Phys. Acoust.*, vol. 27, no. 5, pp. 382–387, Sep.-Oct. 1981.

[11] B. S. Aronov and G. K. Skrebnev, "Effect of the attachment conditions of the piezoceramic plates on the parameters of circular laminated electromechanical transducers," *Sov. Phys. Acoust.*, vol. 29, no. 2, pp. 89–92, Mar.-Apr. 1983.

[12] F. J. Rosato, "Lagrange equations applied to flexural mode transducers," *J. Acoust. Soc. Amer.*, vol. 57, no. 6, pt. 1, pp. 1397–1401, Jun. 1975.

[13] J. B. Greenberg and Y. Stavsky, "Flexural vibrations of certain full and annular composite orthotropic plates," *J. Acoust. Soc. Amer.*, vol. 66, no. 2, pp. 501–508, Aug. 1979.

[14] Y. Stavsky and R. Loewy, "Axisymmetric vibrations of isotropic composite circular plates," *J. Acoust. Soc. Amer.*, vol. 49, no. 5, pt. 2, pp. 1542–1550, May 1971.

[15] A. J. Rudgers, "Acoustical behavior of thick, composite, fluid-loaded plates, calculated using Timoshenko-Mindlin plate theory," Naval Research Laboratory, Washington, D.C., Rep. no. 8317, Nov. 16, 1979.

[16] R. D. Mindlin, "Influence of rotatory inertia and shear on flexural motions of isotropic, elastic plates," *J. Appl. Mechan. Trans. ASME*, vol. 73, pp. 31–38, 1951.

[17] H. F. Tiersten and R. D. Mindlin, "Forced vibrations of piezoelectric crystal plates," *Q. Appl. Math.*, vol. 20, no. 2, pp. 107–119, Jul. 1962.

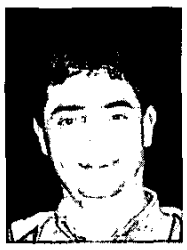

Gökhan Perçin (S'92–M'00) was born in Ezine, Çanakkale, Turkey. He received the B.S. degree in electrical and electronics engineering from Bilkent University, Ankara, Turkey in 1994. He received the M.S. degree in electrical engineering in 1996 and the Ph.D. degree in electrical engineering with minor subject in engineering-economic systems and operations research in 2002, both from Stanford University, California. He worked in Numerical Technologies, Inc., San Jose, California, as a senior software engineer to develop

optical microlithography software. He is cofounder, president, and chief technical officer of ADEPTIENT, Los Altos, California. He has years of experience in the areas of fluid ejection, microfluidics, micromachining, micromachined electromechanical systems, ultrasonic actuators, ultrasound transducers, biomedical imaging, software development, sensors, and actuators. Dr. Perçin is a member of IEEE, IEEE Ultrasonics, Ferroelectrics, and Frequency Control Society, IEEE Electron Devices Society, the Electrochemical Society, and American Vacuum Society. His personal interests include Sufism, the Bektashi Order of Dervishes, photography, swimming, hiking, gourmet cooking, and collecting coins and stamps.

Butrus T. Khuri-Yakub (S'70–S'73–M'76–SM'87–F'95) was born in Beirut, Lebanon. He received the B.S. degree in 1970 from the American University of Beirut, the M.S. degree in 1972 from Dartmouth College, and the Ph.D. degree in 1975 from Stanford University, all in electrical engineering. He joined the research staff at the E. L. Ginzton Laboratory of Stanford University in 1976 as a research associate. He was promoted to Senior Research Associate in 1978 and to Professor of Electrical Engineering (Research) in 1982. He has served on many university committees in the School of Engineering and the Department of Electrical Engineering.

Presently, he is the Deputy Director of the E. L. Ginzton Laboratory. Professor Khuri-Yakub has been teaching both at the graduate and undergraduate levels for over 15 years, and his current research interests include in situ acoustic sensors (temperature, film thickness, resist cure, etc.) for monitoring and control of integrated circuits manufacturing processes, micromachining silicon to make acoustic materials and devices such as airborne and water immersion ultrasonic transducers and arrays, and fluid ejectors, and the field of ultrasonic nondestructive evaluation and acoustic imaging and microscopy.

Professor Khuri-Yakub is a fellow of the IEEE, a senior member of the Acoustical Society of America, and a member of Tau Beta Pi. He is Associate Editor of *Research in Nondestructive Evaluation*, a journal of the American Society for Nondestructive Testing. Professor Khuri-Yakub has authored over 300 publications and has been principal inventor or co-inventor of 52 issued patents. He received the Stanford University School of Engineering Distinguished Advisor Award (June 1987) and the Medal of the City of Bordeaux for contributions to NDE (1983).